Tidevannets innvirkning på tyngdeobservasjoner fra høytliggende kystnære stasjoner

Kristian Breili

Vitenskapelig bedømt (refereed) artikkel

Kristian Breili: Ocean tide loading at elevated coastal gravity stations

KART OG PLAN, Vol 69, pp. 151–164, P.O.B. 5003, NO-1432 Ås, ISSN 0047-3278

High precision geodetic determinations have demonstrated the necessity of ocean tide loading corrections. These corrections are normally obtained by convolving a proper Green's function with an ocean tide model which predicts the tidal heights over all oceans on the Earth's surface. However, published Green's function formulas normally assume an observation point on a spherical Earth and are consequently not appropriate to predict corrections for an elevated observation point. In this paper, Green's function formulas outside a spherical Earth are deduced and used to predict the gravity changes due to ocean tide loading at elevated laboratories along the Norwegian coast. The predictions are compared to gravity observations obtained with the FG5-226 absolute gravimeter in order to illustrate the effect of the modified Green's function.

Key words: Ocean tide loading, Green's function, absolute gravity observations

Kristian Breili, Department of mathematical sciences and technology, Norwegian University of Life Sciences (UMB), P.O.B. 5003, NO-1432 Ås. E-mail: kristian.breili@umb.no

Introduction

The ocean tides induce time dependent loads on the Earth. The phenomenon is called ocean tide loading (OTL) and causes periodic variations in geodetic time series of position estimates, gravity, strain, and tilt. This paper reviews theoretical aspects of the subject and addresses in particular the effect of the vertical height of coastal observation sites.

Generally, the effects of OTL are most prominent in coastal regions where the potential changes due to OTL may reach 10 % of the tidal potential. At the interior of continents, the effect is smaller, but still several percent of the tidal signal (Torge, 2001). The effects of OTL in geodetic time series have been demonstrated by several authors, e.g. Lysaker et al. (2008) and Vey et al. (2002). The first paper analyzed gravity time series from the Norwegian coast and found semi-diurnal OTL-signals with amplitudes reaching 11 µgal. The latter authors observed geometric deformations due to OTL with GPS and reported vertical deformations of 10 cm peak to peak at Brest, France.

The effects of ocean tide loading are usually modeled by combining load Love numbers into Green's functions which are convolved with an ocean tide model over all oceans on the Earth's surface. Mathematically, Green's functions are infinite sums of Love-numbers where Legendre polynomials or their derivatives form weights. They model the Earth's elastic response to the potential which surrounds a unit mass located at a defined spherical distance from the observation point. The effect of the true load is found by scaling the Green's functions with the ocean model.

Green's functions for a spherical Earth are found in e.g. Farrell (1972) and Jentzsch (1997). Both authors sketch briefly how this function is put together, but they do not discuss the situation when the observation point is elevated above sea level. However, gravity stations are seldom situated at sea-level and proper OTL-modeling should take height into account, c.f. Goad (1980), Scherneck (1991), Bos et al. (2002), and Lysaker et al. (2008). In the following sections we address the Green's function for gravity and

present a detailed review of the deduction of a Green's function formula with a height factor. We use the Green's function to predict the gravity effect of OTL and illustrate the importance of taking height into account when the observation point is close to the load, i.e. compare predictions with coastal gravity observations.

A Green's function for gravity outside a spherical Earth

The change ΔV in the gravity potential due to OTL can be decomposed into three components.

$$\Delta V = W - gU + \Phi \tag{1}$$

In Eq. (1), W is the gravitational potential induced by the ocean tides, gU is the change due to vertical displacement of the observation point on the deformed Earth, and Φ is the change due to redistribution of masses of the deformed Earth. The negative sign of the middle term reflects that an upward displacement results in a negative contribution to the potential at the observation point.

The gravity change due to OTL can be modeled by a Green's function which captures all these three components. For an observation point on a spherical Earth, the Green's function for gravity is found in e.g. Farrell (1972) (page 782) and Jentzsch (1997) (page 152)

$$G(\psi) = \frac{g}{M}\sum_{n=0}^{\infty}\left[n + 2h'_n - (n+1)k'_n\right]P_n(\cos\psi) \tag{2}$$

where M is the mass of the Earth, h'_n, k'_n are load Love numbers, and $P_n(\cos\Psi)$ is the nth-degree Legendre polynomial.

The Green's function in Eq. (2) depends only on the spherical distance Ψ and does not include any height term. A Green's function for gravity with a height factor is deduced here. Each component of the gravity OTL-effect is treated separately and finally combined into one formula for the total gravity effect.

The attraction from the ocean tides

The gravitational potential W surrounding a point mass (dm) is described by a scalar function

$$W = \frac{G \cdot dm}{d} \tag{3}$$

where d is the distance between the point mass and the point of observation. The distance d can be expanded into spherical harmonics by the well known formula (see for instance Hofmann-Wellenhof and Moritz (2005), Eq. 1-104.)

$$\frac{1}{d} = \sum_{n=0}^{\infty}\frac{|\mathbf{r}'|^n}{|\mathbf{r}|^{n+1}}P_n(\cos\psi) \tag{4}$$

where $\mathbf{r}$ and $\mathbf{r}'$ are Earth centered radius vectors to the point of observation and the mass, respectively. By letting $\mathbf{r}$ be the vector to the observation point, convergence of the sum in Eq. (4) is ensured for $|\mathbf{r}| \geq |\mathbf{r}'|$, i.e. an observation point located on or exterior to a sphere with radius $|\mathbf{r}'|$. Substitution of Eq. (4) into Eq. (3) expands the gravitational potential into spherical harmonics. We assume a unit load located on a sphere with radius R and write $dm = 1$, $|\mathbf{r}'| = R$ and $G = gR^2/M$.

$$W = \frac{g}{M}\sum_{n=0}^{\infty}\frac{R^{n+2}}{|\mathbf{r}|^{n+1}}P_n(\cos\psi) \tag{5}$$

The change in gravitational acceleration is found by differentiating Eq. (5) along the radius $\mathbf{r}$ through the point of observation.

$$\frac{\partial W}{\partial r} = -\frac{g}{M}\sum_{n=0}^{\infty}(n+1)\left(\frac{R}{|\mathbf{r}|}\right)^{n+2}P_n(\cos\psi) \tag{6}$$

The height of the observation point is defined by setting $|\mathbf{r}| = R + H$. Let also $f^n = (R/(R+H))^n$.

$$\frac{\partial W}{\partial r} = -\frac{g}{M}\cdot\left[\frac{R}{R+H}\right]^2\sum_{n=0}^{\infty}(n+1)\,f^n\,P_n(\cos\psi) \tag{7}$$

When $H << R$ (e.g. $H = 1000$ m), we put safely $(R/(R+H))^2 = 1$.

$$\frac{\partial W}{\partial r} = -\frac{g}{M}\sum_{n=0}^{\infty}(n+1)\,f^n\,P_n(\cos\psi) \tag{8}$$

On the sphere, the height factor f^n equals unity, and Eq. (8) and the first term in Eq. (2) converge to the same function even though the functions seem to be different. This is shown in Appendix B.

The influence on gravity of vertical displacement of the observation point

The vertical displacement causes the observation point to move through the Earth's gravitational field and the potential change is found by multiplying the deformation by the potential's vertical gradient, i.e. the gravitational force. Change in gravitational acceleration is found in a similar manner, i.e. the vertical displacement is multiplied by the vertical gradient of gravity.

$$\Delta g = \frac{\partial g}{\partial r} \cdot U \tag{9}$$

Here, $\partial g/\partial r$ is the gradient of gravity and U the displacement. Density anomalies in the ground close to the observation point are capable of making local vertical free-air gravity gradients deviate significantly from the standard free-air gradient. The standard gradient should be used here, because the density anomalies experience the same displacement as the observation point. A general formula for the standard free-air gradient is found by differentiating Newton's law of gravitation:

$$\frac{\partial g}{\partial r} = \frac{\partial}{\partial r}\left\{\frac{GM}{R^2}\right\} = -2\frac{g}{R} \tag{10}$$

The definition of the Love-numbers in Farrell (1972) connects the deformation's nth-degree coefficient to the load potential's nth-degree coefficient. The total deformation is given by

$$U = \sum_{n=0}^{\infty} U_n P_n(\cos\psi) \tag{11}$$

$$= \sum_{n=0}^{\infty} \frac{h'_n}{g} W_n(r) P_n(\cos\psi) \tag{12}$$

It is reasonable to assume that the displacement at an elevated observation point equals the displacement on the sphere and so $W_n = G/R$ is entered into (12).

$$U = \frac{R}{M}\sum_{n=0}^{\infty} h'_n P_n(\cos\psi) \tag{13}$$

Substitution of Eq. (10) and Eq. (13) into Eq. (9) gives the gravity change due to vertical displacement of the observation point

$$\Delta g = -2\frac{g}{R}\cdot\frac{R}{M}\sum_{n=0}^{\infty} h'_n P_n(\cos\psi)$$

$$= -\frac{g}{M}\sum_{n=0}^{\infty} 2h'_n P_n(\cos\psi) \tag{14}$$

The influence on the Earth's gravity field of crustal deformations

Following Farrell (1972), the nth-degree coefficient of the influence on the Earth's gravity potential of crustal deformations is expressed by

$$\Phi_n(r) = k'_n(r) W_n(r) \tag{15}$$

The total influence is found by adding up coefficients multiplied by Legendre polynomials:

$$\Phi = \sum_{n=0}^{\infty} \Phi_n(r) P_n(\cos\psi) = \sum_{n=0}^{\infty} k'_n(r) W_n(r) P_n(\cos\psi) \tag{16}$$

In Eq. (15) and (16), $W_n(r) = G \cdot R^n/|\mathbf{r}|^{n+1}$ is the nth-degree coefficient of the Legendre polynomials in Eq. (5) and $k'_n(r)$ are load Love numbers of degree n. Then, assuming load Love numbers independent of $\mathbf{r}$,

$$\Phi = G\sum_{n=0}^{\infty} k'_n \frac{R^n}{|\mathbf{r}|^{n+1}} P_n(\cos\psi) \tag{17}$$

Differentiating along $\mathbf{r}$ and putting $G = g\,R^2/M$ yields:

$$\frac{\partial\Phi}{\partial r} = -\frac{g}{M}\sum_{n=0}^{\infty}(n+1)k'_n\left(\frac{R}{|\mathbf{r}|}\right)^{n+2} P_n(\cos\psi) \tag{18}$$

Setting $|\mathbf{r}| = R + H$, and $(R/R + H))^2 = 1$.

$$\frac{\partial\Phi}{\partial r} = -\frac{g}{M}\cdot\sum_{n=0}^{\infty}(n+1)\,k'_n f^n P_n(\cos\psi) \tag{19}$$

The total Green's function

The total change in gravity acceleration due to OTL is found by combining Eq. (8), Eq. (14), and Eq. (19) into one Green's function

$$G(\psi, H) =$$

$$\frac{g}{M}\sum_{n=0}^{\infty}\left[-\left((n+1)+(n+1)k'_n\right)f^n + 2h'_n\right]P_n(\cos\psi), \tag{20}$$

where $f^n = (R/R+H))^n$. In the deduction of Eq. (20), H was the height of the observation point above the sphere. For practical applications, H represents the height above sea level. Compared to Eq. (2), two terms in Eq. (20) are multiplied by a height dependent factor f^n. Thus, the formula is also valid for elevated observation points. Note the sign convention used in Eq. (2) and Eq. (20). To obtain a positive gravity change in the downward direction (as recorded by a gravimeter), the sign must be reversed.

The Green's function in Eq. (20) involves summation of load Love numbers and Legendre polynomials up to infinite degrees. For practical calculations, truncation is necessary. Problems arise because the sum is not well behaved. The problem is solved by factoring out analytical expressions for the asymptotic terms. The remaining sums are well behaved and can be truncated at e.g. n = 10000. This more efficient computational scheme is deduced in Appendix A.

The effect of an elevated observation point

Green's functions for the attraction component are graphically illustrated in Fig. 1 (left). The figure shows the attraction from a unit point mass located at spherical distances between 0.001° and 180° from the observation point. Four cases are considered, i.e. observation points at 1000 m (solid line), 100 m (dashed line), 10 m (dash-dotted line), and at sea level (dotted line). The functions are scaled by the attraction at an observation point at sea level. This implies that the scaled Green's function for attraction at sea level is always unity in the left panel of Fig. 1.

For elevated observation points, the height effect is considerable for observation points close to the load, e.g. the attraction from a unit load located at a spherical distance of 0.001° from an observation point at height 1000 m is ~1000 times larger than a corresponding observation point at sea level.

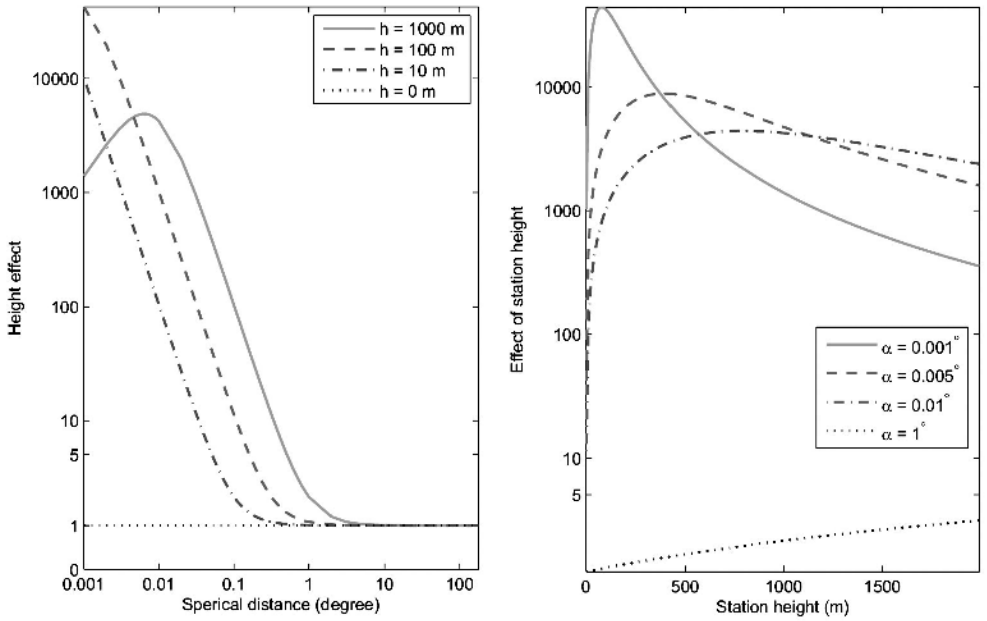

Fig. 1. Left panel: The Green's function for attraction from the ocean tides. Four examples are considered, i.e. an observation point at h = 1000 m (solid line), h = 100 m (dashed line), h = 10 m (dash-dotted line), and at sea level (dotted line). The Green's functions are scaled by the attraction at sea level. Right panel: The height effect as function of the height of the observation point. The unit load was located at four different spherical distances, i.e. at 0.001° (solid line), 0.005° (dashed line), 0.01° (dash-dotted line), and 1° (dotted line).

The height effect diminishes for increasing distances. For the examples in the present analysis, the effect is close to zero for spherical distances larger than 1–5º. The decay rate depends on the height of the observation point. In general, the height effect decays more slowly as height increases.

Figure 1 (right) shows that the height effect reaches a maximum when the distance to the load is approximately equal to the station height. For spherical distances of 0.001º (~100 m), 0.005º (~500 m), and 0.01º (~1100 m), the largest effect is found for station heights of 80 m, 400 m, and 800 m, respectively. For larger distances to the load, the height effect grows steadily with increasing height

Green's functions for the gravity change due to crustal deformations are graphically illustrated in the left panel of Fig. 2. The same four examples are considered and the functions are scaled by the corresponding effect at sea level. The pattern found in Fig. 2 is different from that of the attraction component. Firstly, the height effect has a smaller maximum than the attraction component. Secondly, the load effect declines with increasing height, e.g. for an observation point at a height 100 m and at spherical distance 0.001º from the load, the effect of this OTL component is ~75 % of the effect at sea level. A slight increase of the load effect occurs for spherical distances between 0.1 to 0.5º. The increase is small, reaching only 5 % for the examples considered here. In the right panel of Fig. 2 the height effect is calculated for loads at four spherical distances and for observation points at heights between 0 and 2000 m. For the spherical distances 0.001º and 0.01º, the height effect grows with increasing height, i.e. the gravity change due to crustal deformations is reduced with increasing height. The opposite is found for a load located at a spherical distance of 0.1º from the observation point. At spherical distances of 1º or more, the load effect is independent of the height of the observation point.

For most applications, the height factor of the elastic part (vertical displacement and crustal deformations) of the Green's function is negligible. Nevertheless, the height factor for the attraction component is included in most software packages computing OTL corrections, e.g. the OTL service at *http://www.oso.chalmers.se/~loading/* (Scherneck and Bos, 2006), the SPOTL package (Agnew, 2005) and the g-software provided by Micro-g Solutions Inc.

Comparison with gravity observations

To analyze the actual effect of a height factor, the formulas in Appendix A were used to calculate Green's functions which were convolved with an ocean tide model. Usually, the ocean is divided into a grid and the ocean model defines the tidal height for each grid point. This transforms the convolution integral into a sum over a finite number N of ocean cells:

$$I(\varphi,\lambda,H,t) = \rho_w \sum_{i=1}^{N} G(\psi_i,H)\, O(\varphi'_i,\lambda'_i,t)\, dS_i \quad (21)$$

In Eq. (21) I is the OTL-effect at a point (φ,λ,H) at epoch t, ρ_w is the density of seawater, $G(\Psi_i,H)$ is the Green's function for a spherical distance Ψ_i and a observation point at height H, O is the ocean model which gives the tidal height at a point φ',λ' at epoch t, and dS_i is the area of ocean cell i. Equation (21) is in accordance with Francis and Mazzega (1990).

The NAO99b ocean tide model (Matsumoto et al, 2000) was downloaded from *http://www.miz.nao.ac.jp/staffs/nao99/index_EN.html* and the eleven tidal constituents M2, S2, N2, K2, K1, O1, P1, Q1, MM, Mf, and Ssa (see Chap. 4.3 in Lambeck (1988) for a brief description of the tidal constituents) were included in the calculations of the ocean tides. The NAO99b model is available on a 0.5º x 0.5º grid. For OTL-modeling, refinement of the ocean model is quite important in coastal regions close to the observation point because a significant part of a coastal ocean cell is likely to cover land areas. In this analysis, the ocean model was refined onto a 0.05º x 0.05º grid within 1º from the observation point and onto a 0.002º x 0.002º grid within 0.1º from the observation point. A high resolution coastline from the Global Self-consistent, Hierarchical, High-resolution Shoreline Database (GSHHS) (Wessel and Smith, 1996) was downloaded from *http://www.ngdc.noaa.gov/mgg/shorelines/gshhs.html*

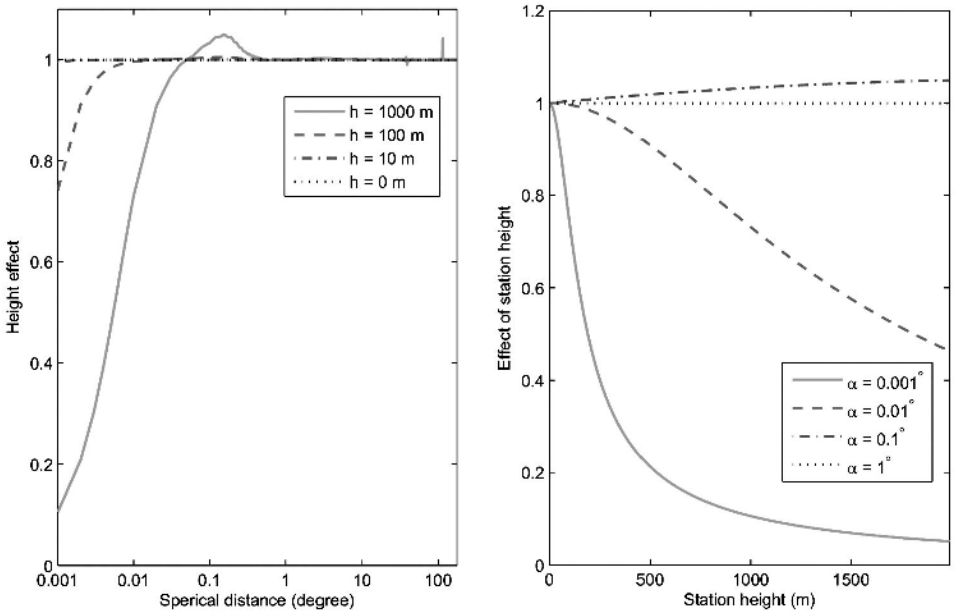

Fig. 2. Left panel: The Green's function for the gravity change due to crustal deformations. Four examples are considered, i.e. an observation point at h = 1000 m (solid line), h = 100 m (dashed line), h = 10 m (dash-dotted line), and at sea level (dotted line). The Green's functions are scaled by the load effect at sea level. The spike found close to a spherical distance of 100° is an artifact due to the scaling. Right panel: The height effect as function of the height of the observation point. The unit load was located at four different spherical distances, i.e. at 0.001° (solid line), 0.01° (dashed line), 0.1° (dash-dotted line), and 1° (dotted line).

and used to distinguish between land and sea. Green's functions were calculated by using load Love numbers for the Preliminary Reference Earth Model (PREM) (Dziewonski and Anderson, 1981) up to a maximum degree of 10000. These numbers were determined by spline interpolation of the tabulated values in Jentzsch (1997).

Modeled gravity changes due to OTL were compared to gravity observations collected at Andøya, Bodø, Tromsø, and Ålesund by the FG5-226 absolute gravimeter. In order to isolate the OTL-effect, the gravity observations were corrected for Earth tides, polar motion, and atmospheric loading with the g-software (g Users Manual v5.0, 2005). The Earth tides were calculated from a tide generating potential from Tamura (1987) and Love numbers of the Wahr-Dehant-Defraign model (Dehant et al. 1999). Additionally, the mean of the time series was subtracted because only relative gravity changes are of relevance in this analysis. A detailed description of the instrument is found in Niebauer et al. (1995) and processing and observational procedures are described in Lysaker et al. (2008). The coordinates of the stations are found in Table 1 and the geographical locations are illustrated in Fig. 3. The station heights and distances to the sea are also found in Table 1. All stations are located within 2 km from the Norwegian coast and are considered to be elevated stations.

Figure 5 shows observations and two predicted time series of the gravity effects due to OTL for stations in Fig. 3. For each station, two Green's functions were generated, one for sea level (dashed line), and one for the actual height of the observation point (solid line).

Table 1. Coordinates and orthometric heights of the gravity stations.

Station	Latitude	Longitude	Height	Dist. to sea
Andøya	69.2780º N	16.0087º E	370 m	1.3 km
Bodø	67.2875º N	14.4340º E	68 m	2.0 km
Tromsø	69.6628º N	18.9397º E	102 m	1.1 km
Ålesund	62.4762º N	6.1985º E	140 m	0.2 km

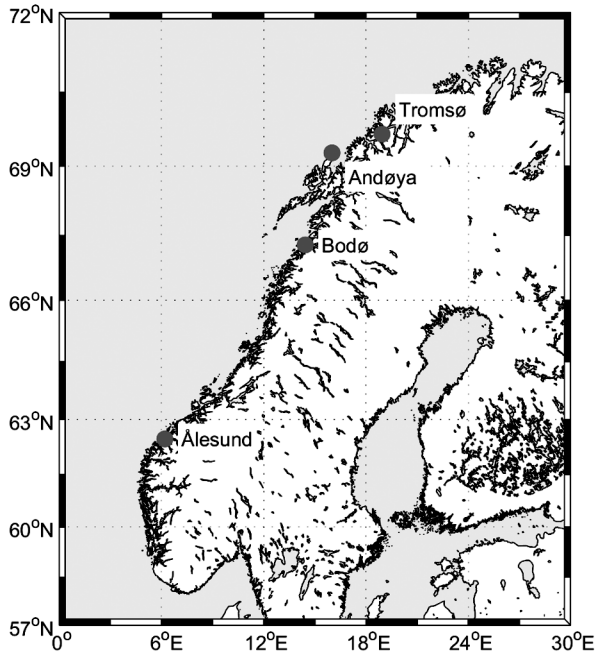

Fig. 3. The gravity stations used to analyze the effect of a Green's function with a height factor.

Andøya

The gravity laboratory at Andøya is located at a height of 370 m on an island facing the Norwegian Sea. The distance to the coast is 1.3 km. Within 30–50 km from the gravity laboratory there are no large islands or winding fiords. The need for proper treatment of the station height is clearly illustrated by the two predicted OTL models. They differ by about 5 μgal at OTL maximum. The RMS reduction (Table 2) is 52 % for the OTL model designed for sea level and 87 % for the OTL model which includes the height factor. Also, this OTL model removes all periodic variations in the gravity time series. Hence, a remarkably good fit is obtained between the observations and the OTL model when the height factor is included.

Bodø

Bodø is located 2.0 km from the ocean on a small hill, 68 m above sea level. Bodø is the lowest station in this study and is located farthest from the coast. The NAO99b model was used without any modifications in Bodø. The second panel (from above) of Fig. 5 shows that there are no significant deviations between the two OTL models. Approximately the same RMS reduction is obtained by both models, i.e. 49 % for the model with the height factor and 44 % for the model for sea level. Except for a low minimum on day 196, both models fit the observations well. The origin of the outlying observations is at present not known. In summary, the height factor is of minor importance in Bodø.

Tromsø

The gravity laboratory in Tromsø is located on an island, 102 m above sea level and 1.1 km from the coast. The island is located in the middle of a fiord. This implies relatively small tidal basins close to the laboratory and a limited attraction component from the local ocean tides. Consequently, the OTL signal is expected to be weaker in Tromsø than at stations facing the open sea. This is seen in the third panel (from above) of Fig 5. Deviations of 2–3 μgal are found between the two OTL models in Tromsø. The model tailored to the station's height fits the observations best. It reduces the gravity time series RMS by 58 % compared to 53 % for the OTL model at sea level.

Ålesund

Ålesund is located on a peninsula at the mouth of Storfjorden in Norway. The peninsula is surrounded by several islands and fiords making the figure of the local coastline complex. The gravity laboratory is located at a horizontal distance of 200 m from the ocean and 140 m above sea level.

Before convolving the NAO99b ocean tide model with the Green's functions, the ocean tide model was modified in the area close to Ålesund. This was necessary because the ocean tides within 10 km from the observation point are not included in the original model. Lysaker et al. 2008 showed that it is of vital importance to include the local ocean tides for proper calculation of the attraction component. Thus, a new grid point was added at 6.25° E 62.25° N. The ocean tides at the new grid point was found by adopting the NAO99b tidal constituents for the grid point at 5.75° E 62.25° N. Tidal heights computed from these coefficients were compared to tide gauge observations in Ålesund, see Fig. 4. For the epochs coincident with the FG5 observations, the overall fit is good. The standard deviation is 8.8 cm and the maximum deviation is 20 cm. Ocean tides of corresponding heights create gravitational attraction of 0.5 μgal and 1.2 μgal, respectively. Thus, the expansion of the NAO99b ocean tide model is considered to be a sufficiently accurate representation of the ocean tides within 5–10 km from the observation point.

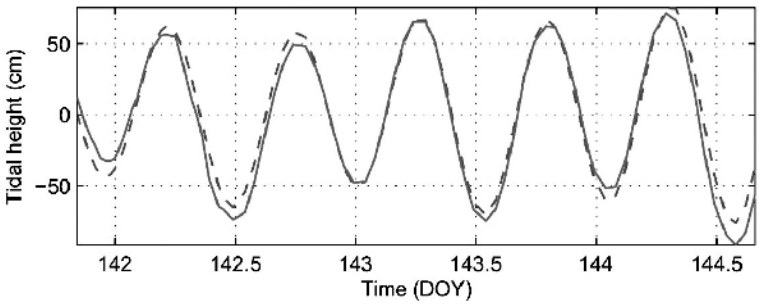

Fig. 4. Comparison of predicted tidal heights from NAO99b (dashed line) and tides observed with the tide gauge in Ålesund (solid line). The NAO99b predicted tidal heights are computed from tidal constituents at 5.75° E 62.25° N.

The lower panel of Fig. 5 shows significant deviation between gravity observations and the OTL model calculated from the Green's function at sea level. Better fit to the observations was obtained by using the Green's function with a height factor. The same pattern is reflected by the RMS values listed in Table 2. The OTL model which includes the height factor reduces the RMS by 50 % while the OTL model at sea level reduces the RMS by 21 %. We notice that some of the observations in the gravity series in Ålesund deviate significantly from both OTL models. The origin of this variation is at present unknown.

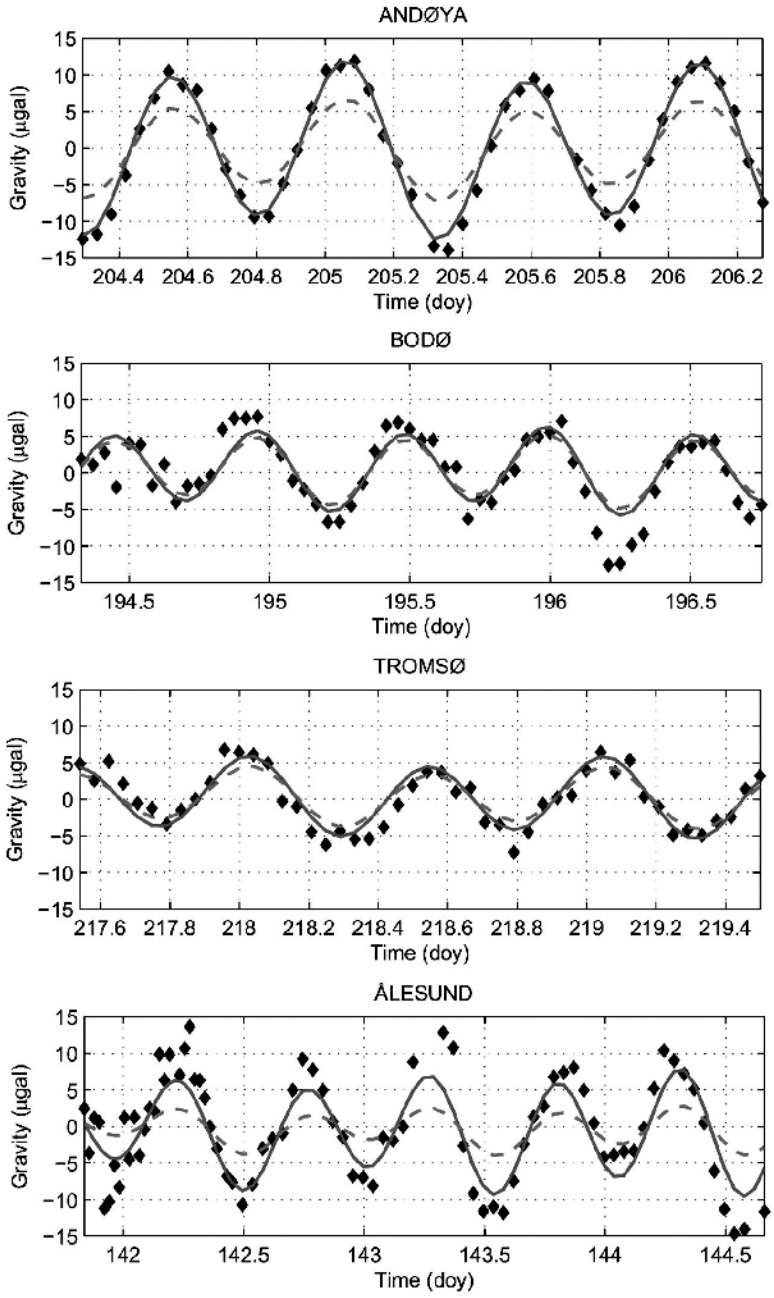

Fig. 5. Time series of observed gravity residuals with no OTL corrections are shown as diamonds for Andøya, Bodø, Tromsø, and Ålesund, Norway. Modeled OTL effects are shown as solid lines (with height factor) and dashed lines (without any height factor). The importance of proper height modeling for an elevated observation point close to the sea is evident.

Table 2. RMS of the gravity time series with and without OTL corrections. Two OTL models were computed. One based on a Green's function with a height factor (Model 1), and one based on a Green's function at sea level (Model 2).

Station	No OTL-corrections	Model 1	Model 2
Andøya	8.0 µgal	1.1 µgal	3.8 µgal
Bodø	5.1 µgal	2.6 µgal	2.8 µgal
Tromsø	3.8 µgal	1.6 µgal	1.8 µgal
Ålesund	7.8 µgal	3.9 µgal	6.2 µgal

Discussion

The percentage contribution from each OTL component was calculated for the OTL models at sea level and at the height of the stations. The ratios were estimated by summing up the amplitudes from each tidal constituent. Then the sum was divided by the total sum of all amplitudes:

$$\text{Contribution from component } j = \frac{\sum_{i=1}^{11} A_j^i}{\sum_{i=1}^{11}\sum_{j=1}^{3} A_j^i} \cdot 100\,\% \qquad (22)$$

In Eq. (22) the OTL component (attraction, displacement, and the gravitational effect of crustal deformations, cf. Eq. (1)) is assigned by the index j, and A_j^i is OTL constituent i of component j. Equation (22) does not take into account phase relationships between the constituents and the components. Thus, the estimated ratios should be considered as approximate estimates of each component's contribution to the total OTL signal.

The results are shown in Table 3. It is evident that proper height treatment is crucial for modeling the attraction component of coastal stations. At station height, the percentage contribution from the attraction component makes a significant part of the total OTL signal at all stations. The situation is different at sea level, where the attraction component is the weakest of the three components. The height factor influences the attraction from the local tides most strongly, and it is therefore most important to correctly model the attraction from the local tides surrounding an elevated gravity laboratory.

Table 3. The percentage contribution from each OTL effect at station height and sea level.

Station	Height	Attraction	Displacement	Crustal deformations
Andøya	370 m	42.3 %	46.6 %	11.1 %
	sea level	11.8 %	71.2 %	17.0 %
Bodø	68 m	22.7 %	63.2 %	14.0 %
	sea level	12.1 %	71.9 %	18.0 %
Tromsø	102 m	30.4 %	56.3 %	13.2 %
	sea level	13.0 %	70.4 %	16.5 %
Ålesund	140 m	58.4 %	34.9 %	6.7 %
	sea level	8.0 %	77.2 %	14.8 %

The effect of the height factor is largest in Ålesund and at Andøya. This can be explained as the effect of relatively large local tidal basins and the relationship between the station height and distance to the ocean. The effect is especially prominent in Ålesund, where the distance to the ocean is approximately the same as the laboratory's height above sea level. This corresponds to the relationship found in the right panel of Fig. 1. The effect of a Green's function tailored the station's height is not so prominent at Tromsø and Bo-

dø. In Tromsø this can be explained by small local tidal basins and in Bodø by the modest height of the station.

Conclusion

A Green's function for gravity with a height factor was deduced. The station's height affects the OTL signal through two components, i.e. the attraction component and the gravity change due to crustal deformations. The largest effect is found for the first component and for most applications the effect is negligible for the latter component.

Graphical representations of the Green's function show that it is important to include the height factor when the spherical distance between the observation point and the load is small. For the attraction component, it was found that the effect of the station height is largest when the distance to the ocean is approximately equal to the station's height. For distances larger than about 1-5° the height effects are much smaller and need not be taken into account for proper modeling of gravity changes due to OTL.

The deduced Green's function was used to predict gravity changes due to OTL and the predictions were compared to gravity observations at Andøya, Bodø, Tromsø, and Ålesund. The Green's function with the height factor improves the OTL model. This was illustrated by using the predictions to correct the gravity observations for OTL. The RMS was significantly reduced when the Green's functions with the height factor were used. The examples clearly illustrated the need for a height factor for elevated gravity laboratories close to the ocean.

Acknowledgements

I am indebted to Olav Mathisen, Dagny I. Lysaker, and Bjørn R. Pettersen for useful and interesting discussions. Gravity observations at Andøya were made by Ove C. D. Omang.

Appendix A: Expansions of the Green's function for practical calculations

The Newtonian attraction

The attraction term in Eq. (8) is:

$$\frac{\partial W}{\partial r} = -\frac{g}{M}\sum_{n=0}^{\infty}(n+1)f^n P_n(\cos\psi) \tag{23}$$

Manipulation of the sum yields:

$$\begin{aligned}\frac{\partial W}{\partial r} &= -\frac{g}{M}\cdot\frac{\partial}{\partial f}\left\{\sum_{n=0}^{\infty} f^{n+1}P_n(\cos\psi)\right\} \\ &= -\frac{g}{M}\cdot\frac{\partial}{\partial f}\left\{f\sum_{n=0}^{\infty} f^n P_n(\cos\psi)\right\}\end{aligned} \tag{24}$$

From Eq. 1-103 in Hofmann-Wellenhof and Moritz (2005) an analytical expression for the term inside the brackets in Eq. (24) is adopted.

$$\begin{aligned}&\sum_{n=0}^{\infty}\alpha^n P_n(u) = \frac{1}{\sqrt{1-2\alpha u+\alpha^2}} \\ &\Rightarrow f\sum_{n=0}^{\infty} f^n P_n(\cos\psi) = \frac{f}{\sqrt{1-2f\cos\psi+f^2}}\end{aligned} \tag{25}$$

A final analytical expression for the attraction term is obtained by differentiating Eq. (25) with respect to f, and by setting $f = R/(R + H)$ and $r = R + H$.

$$\frac{\partial W}{\partial r} = -\frac{g\,r^2}{M}\left[\frac{r - R\cos\psi}{(r^2 - 2r\,R\cos\psi + R^2)^{3/2}}\right] \tag{26}$$

The vertical displacement

The gravitational effect of vertical displacement is from Eq. (14):

$$\delta g = -\frac{g}{M}\sum_{n=0}^{\infty} 2h'_n P_n(\cos\psi) \tag{27}$$

Manipulation of the sum yields two sums:

$$\delta g = -\frac{2g}{M}\sum_{n=0}^{\infty}(h'_\infty - h'_\infty + h'_n)P_n(\cos\psi)$$

$$= -\frac{g}{M}\left[2h'_\infty\sum_{n=0}^{\infty}P_n(\cos\psi) + 2\sum_{n=0}^{\infty}(h'_n - h'_\infty)P_n(\cos\psi)\right] \tag{28}$$

An analytical function for the first sum is found in Farrell (1972):

$$\sum_{n=0}^{\infty}P_n(\cos\psi) = \frac{1}{2\sin(\psi/2)} \tag{29}$$

The second sum is well behaved and may be truncated for e.g. degree n = 10000.

$$\delta g = -\frac{g}{M}\left[\frac{h'_\infty}{\sin(\psi/2)} + 2\sum_{n=0}^{\infty}(h'_n - h'_\infty)P_n(\cos\psi)\right] \tag{30}$$

The change in Earth's potential

The sum in Eq. (19) is separated into two sums.

$$\frac{\partial\Phi}{\partial r} = -\frac{g}{M}\sum_{n=0}^{\infty}(n+1)k'_n f^n P_n(\cos\psi)$$

$$= -\frac{g}{M}\left[\sum_{n=0}^{\infty}n\,k'_n f^n P_n(\cos\psi) + \sum_{n=0}^{\infty}k'_n f^n P_n(\cos\psi)\right] \tag{31}$$

Both sums in Eq. (31) are manipulated into well behaved sums. First sum of Eq. (31):

$$\sum_{n=0}^{\infty}n\,k'_n f^n P_n(\cos\psi) = \sum_{n=0}^{\infty}\left[k'_\infty - k'_\infty + n\,k'_n\right]f^n P_n(\cos\psi)$$

$$= k'_\infty\sum_{n=0}^{\infty}f^n\,P_n(\cos\psi) + \sum_{n=0}^{\infty}(n\,k'_n - k'_\infty)f^n\,P_n(\cos\psi)$$

$$= \frac{k'_\infty}{\sqrt{1-2f\cos\psi+f^2}} - k'_\infty + \sum_{n=1}^{\infty}(n\,k'_n - k'_\infty)f^n\,P_n(\cos\psi) \tag{32}$$

Second sum of Eq. (31) is first manipulated by changing the limits of summation. Because k'_0 = 0 the summation is set to start at n = 1:

$$\sum_{n=0}^{\infty}k'_n f^n\,P_n(\cos\psi) = \sum_{n=1}^{\infty}k'_n f^n P_n(\cos\psi) \tag{33}$$

Then the sum in Eq. 33 is split into two sums in a similar manner as the first sum of Eq. (31):

$$= \sum_{n=1}^{\infty}\frac{1}{n}\left[k'_\infty - k'_\infty + n\,k'_n f^n\right]P_n(\cos\psi)$$

$$= k'_\infty\sum_{n=1}^{\infty}\frac{1}{n}P_n(\cos\psi) + \sum_{n=1}^{\infty}\frac{1}{n}(n\,k'_n f^n - k'_\infty)P_n(\cos\psi) \tag{34}$$

Khan (2005) gives an analytical expression for the sum in the first term of Eq. (34):

$$\sum_{n=1}^{\infty} \frac{1}{n} P_n(\cos\psi) = -\log\left[\sin(\frac{\psi}{2}) + \sin^2(\frac{\psi}{2})\right] \tag{35}$$

Equation (35) inserted into Eq. (34):

$$\sum_{n=0}^{\infty} k'_n f^n P_n(\cos\psi) =$$

$$-k'_\infty \log\left[\sin(\psi/2) + \sin^2(\psi/2)\right] + \sum_{n=1}^{\infty} \frac{1}{n}(n\,k'_n f^n - k'_\infty) P_n(\cos\psi) \tag{36}$$

Substitution of the expressions in Eq. (32) and (36) into Eq. (31) gives the final expression for the change in Earth's potential. The sum is well behaved because the asymptotic part of the sum is factorized out. The sum can be truncated for e.g. n = 10000.

$$\frac{\partial\Phi}{\partial r} = \frac{g\,k'_\infty}{M}\left(1 + \log\left[\sin(\psi/2) + \sin^2(\psi/2)\right] - \frac{1}{\sqrt{1 - 2f\cos\psi + f^2}}\right)$$

$$-\frac{g}{M}\sum_{n=1}^{\infty}\left[(n\,k'_n - k'_\infty)f^n + \frac{1}{n}(n\,k'_n f^n - k'_\infty)\right] P_n(\cos\psi) \tag{37}$$

Appendix B: Convergence of the attraction term

On the sphere, Eq. (8) converges to the same function as the first term of Eq. (2). This is demonstrated here by finding the function of convergence for the two terms. To do this, two identities from Appendix 1 in Farrell (1972) are useful:

$$\sum_{n=0}^{\infty} n\,P_n(\cos\psi) = -\frac{1}{4\sin(\psi/2)} \tag{38}$$

$$\sum_{n=0}^{\infty} P_n(\cos\psi) = \frac{1}{2\sin(\psi/2)} \tag{39}$$

The first term of Eq. (2) is identical to Eq. (38) multiplied with g/M.
On the sphere, $f^n = 1$ and Eq. (8) can be written

$$-\frac{g}{M}\sum_{n=0}^{\infty}(n+1)P_n(\cos\psi)$$

$$= -\frac{g}{M}\left[\sum_{n=0}^{\infty} n\,P_n(\cos\psi) + \sum_{n=0}^{\infty} P_n(\cos\psi)\right] \tag{40}$$

Equation (38) and (39) inserted into Eq. (40) results to:

$$-\frac{g}{M}\left[-\frac{1}{4\sin(\psi/2)} + \frac{1}{2\sin(\psi/2)}\right]$$

$$= -\frac{g}{M}\cdot\frac{1}{4\sin(\psi/2)} \tag{41}$$

Thus, Eq. (8) agrees with the first term of Eq. (2) on the sphere.

References

Agnew D.C. (2005). SPOTL: Some Programs for Ocean-Tide Loading. Institute of Geophysics and Planetary Physics, Scripps Institution of Oceanography, University of California, Last visited 2009.07.01 http://www.igpp.ucsd.edu/eagnew/spotldocs.pdf.

Bos M., Baker T., Røthing K. and Plag H.P. (2002). Testing ocean tide models in the Nordic seas with tidal gravity observations. Geophysical Journal International, **150**, pp 687–694.

Dehant V., Defraigne P. and Wahr J.M. (1999). Tides for an Earth in a non-hydrostatic equilibrium. Journal of Geophysical Research, **104 (B1)**, pp 1035–1058.

Dziewonski A.D. and Anderson D.L. (1981). Preliminary reference earth model. Phys Earth Planet Inter, **25**, pp 297–356.

Farrell W.E. (1972). Deformation of the Earth by Surface Loads. Reviews of Geophysics and Space Physics, **10**, pp 761–797.

Francis O. and Mazzega P. (1990). Global charts of ocean tide loading effects. Journal of Geophysical Research, **95**, pp 11,411–11,424.

g Users Manual v5.0 (2005). Micro-g Solutions Inc., Erie, Colorado, USA.

Goad C.C. (1980). Gravimetric Tidal Loading Computed From Integrated Green's Functions. Journal of Geophysical Research, **85(B5)**, pp 2679–2683.

Hofmann-Wellenhof B. and Moritz H. (2005). Physical Geodesy, 1st edn. SpringerWienNewYork.

Jentzsch G. (1997). Earth Tides and Ocean Tidal Loading. Lecture Notes in Earth Sciences, **66**, pp 145–171.

Khan S. A. (2005). Surface deformations analyzed using GPS time series. PhD thesis, Danish National Space Center.

Lambeck K. (1988). Geophysical Geodesy. The Slow Deformations of the Earth, 1st edn. Oxford University Press.

Lysaker D. I., Breili K. and Pettersen B.R. (2008). The gravitational effect of ocean tide loading at high latitude coastal stations in Norway. Journal of Geodesy, **82**, pp 569–583.

Matsumoto K., Takanezawa T. and Ooe M. (2000). Ocean Tide Models Developed by Assimilating TOPEX/POSEIDON Altimeter Data into Hydrodynamical Model: A Global Model and a Regional Model around Japan. Journal of Oceanography, **56**, pp 567– 581.

Niebauer T.M., Sasagawa G.S., Faller J.E., Hilt R. and Klopping F. (1995). A new generation of absolute gravimeters. Metrologia, **32**, pp 159–180.

Scherneck H. G. (1991). A parameterized solid earth tide model and ocean tide loading effects for global geodetic baseline measurements. Geophysical Journal International, **106**, pp 677–694.

Scherneck H. G. and Bos M. (2006). The ocean tide loading provider. Last visited 2009.07.01 http://www.oso.chalmers.se/~loading.

Tamura Y. (1987). A Harmonic Development of the Tide-Generating Potential. Marées Terrestres Bulletin D'Informations, **99**, pp 6813–6855.

Torge W. (2001). Geodesy, 3rd edn. Walter de Gruyter.

Vey S., Calais E., Llubes M., Florsch N., Woppelmann G., Hinderer J., Amalvict M., Lalancette M.F., Simon B., Duquenne F. and Haase J.S. (2002). GPS measurements of ocean loading and its impact on zenith tropospheric delay estimates: a case study in Brittany, France. Journal of Geodesy, **76**, pp 419–427.

Wessel P. and Smith W.H.F. (1996). A Global Self-consistent, Hierarchical, High-resolution Shoreline Database. Journal of Geophysical Research, **101**, pp 8741–8743.